Features of polymerization of methylmethacrylate using a photocatalyst – the complex oxide RbTe1.5W0.5O6

Liudmila Leonidovna Semenycheva (llsem@yandex.ru)
Lobachevsky State University of Nizhny Novgorod https://orcid.org/0000-0003-3413-2899
Victoria Chasova
Lobachevsky State University of Nizhny Novgorod
Julia Matkivskaya
Lobachevsky State University of Nizhny Novgorod
Diana Fukina
Lobachevsky State University of Nizhny Novgorod
Andrey Koryagin
Lobachevsky State University of Nizhny Novgorod
Tatiana Belaya
Lobachevsky State University of Nizhny Novgorod
Alexandra Grigoreva
Lobachevsky State University of Nizhny Novgorod
Yuri Kursky
Lobachevsky State University of Nizhny Novgorod
Evgeny Suleimanov
Lobachevsky State University of Nizhny Novgorod

Original Research Full Papers

Keywords: methylmethacrylate, complex oxide RbTe1.5W0.5O6, photocatalysis, pectin, polymerization

Posted Date: January 30th, 2021

DOI: https://doi.org/10.21203/rs.3.rs-161298/v1

Features of polymerization of methylmethacrylate using a photocatalyst – the complex oxide $RbTe_{1.5}W_{0.5}O_6$

Abstract

Radical polymerization of methylmethacrylate in an aqueous emulsion was carried out using the complex oxide $RbTe_{1.5}W_{0.5}O_6$ as a photoinitiator under visible light irradiation with λ= 400-700 nm. Studies of the process and reaction products using modern methods of physical and chemical analysis (GPC, IR, NMR, etc.) have shown that several directions of monomer transformations occur simultaneously in the reaction mixture. Polymethylmethacrylate, produced in the organic phase and characterized by Mn ~ 140-145 kDa, is a result of polymerization initiation by a hydroxyl radical formed due to complex transformations of electron-hole pairs during irradiation of the photocatalyst. Moreover, the interaction of the hydroxyl radical with OH groups on the complex oxide $RbTe_{1.5}W_{0.5}O_6$ surface and the subsequent formation of oxygen-centered radicals lead to grafting polymer macromolecules onto the photocatalyst surface. In addition, methylmethacrylate is able to oxidize to a cyclic dimer with terminal double bonds and then form a polymer with cyclic dimer links due to coordination by double bonds on the complex oxide $RbTe_{1.5}W_{0.5}O_6$ surface. The high activity of the hydroxyl radical made it possible to obtain the graft copolymer PMMA-pectin by grafting the polymer product onto the surface of the natural polymer-pectin. Comparison of the sponge morphology of the graft copolymer PMMA-pectin and the initial pectin samples using the scanning electron microscopy method showed a noticeable difference in their structural and topological organization. This fact is especially interesting in terms of studying the properties of the graft copolymer as a material for the scaffolds.

Keywords: methylmethacrylate, complex oxide $RbTe_{1.5}W_{0.5}O_6$, photocatalysis, pectin, polymerization

1 Introduction

The creation of new effective photocatalysts attracts the attention of scientists as a direction of research involving waste-free technologies. Photoinitiators are an alternative to traditional initiators of radical polymerization process. The photocatalytic water splitting with the formation of hydrogen and organic compounds decomposition in aqueous solutions to carbon dioxide and water suggest either direct interaction with reactive hydroxyl radicals formed as a result of complex transformations of electron-hole pairs, or with oxidizing centers on the photocatalyst surface [1-10]. The formation of an active hydroxyl radical in the reaction system is of interest for organic synthesis, primarily for the production of new polymer materials without material initiators fragments with organic nature [9, 11]. The complex oxide $RbTe_{1.5}W_{0.5}O_6$ with β-pyrochlore structure has been synthesized recently. A detailed study of its electronic structure showed the fundamental possibility of using it as a photocatalyst under visible light irradiation (λ= 400-700 nm), and the photocatalytic oxidizing of methylene blue on the $RbTe_{1.5}W_{0.5}O_6$ surface has been experimentally confirmed [7, 12].

The aim of this work is to identify the features of radical polymerization using complex oxide $RbTe_{1.5}W_{0.5}O_6$ as a photoinitiator under visible light irradiation λ= 400-700 nm on the example of a monomer – methylmethacrylate (MMA) and to characterize the most important properties of the resulting polymer products.

2 Experimental Section

2.1 Materials

Commercial organic solvents: chloroform, toluene, etc. were pre-purified according to conventional methods, MMA was pre-purified from the stabilizer, and pectin Unipectine PG DS (Cargill, Germany, France) was used.

2.2 Preparation of the $RbTe_{1.5}W_{0.5}O_6$ photocatalyst

Polycrystalline sample of the $RbTe_{1.5}W_{0.5}O_6$ was prepared by solid-state reaction using the method described in previous work [12]. Prepared powder sample was grounded in planetary mill for ~16-18 hours with speed 30 min^{-1} to reach minimal size of participles. Phase individuality of synthesized sample has been confirmed by powder X-ray diffraction (XRD) analysis. Figure 1a presents the $RbTe_{1.5}W_{0.5}O_6$ diffraction pattern, which can be indexed in cubic system with space group $Fd\bar{3}m$ [13]. Comparison of the obtained X-ray diffraction pattern and the theoretical one,

calculated from the single-crystal X-ray structural data, indicates the monophasic nature of the powder. Impurity phases have not been detected within the sensitivity of the method.

The morphology of $RbTe_{1.5}W_{0.5}O_6$ powder has been investigated by scanning electron microscopy (SEM) method and shown in Fig. 2a. The powder contains different size particles with average size of 736 nm (Fig. 1b). However the particles size distribution has small maximum about of 1.4 μm that can be explained by formation of stable agglomerates consisted of nanosized particles, which hardly destroyed under ultrasonic condition.

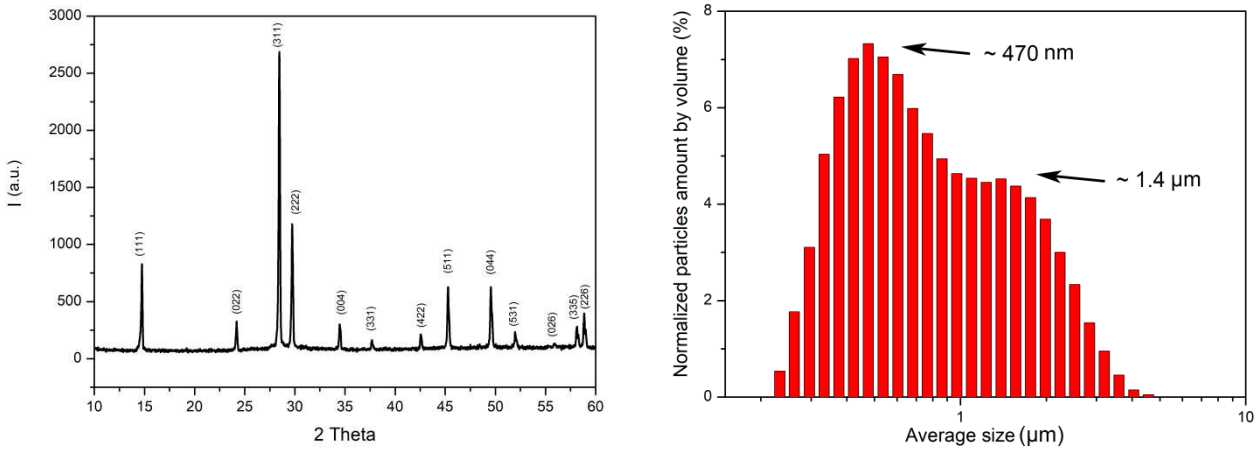

a **b**

Fig. 1 X-ray powder diffraction pattern (**a**) and size particles distribution by volume over the size of $RbTe_{1.5}W_{0.5}O_6$ (**b**)

2.3 Preparation of the emulsion

The MMA emulsion was prepared by mixing $RbTe_{1.5}W_{0.5}O_6$ powder and liquid components. Water and monomer was in a ratio of 75:25 with the addition of "Ediscan" and tetraethylene glycol dimethyl ether (TEGDME) emulsifiers. The MMA emulsion with pectin was prepared similarly by mixing $RbTe_{1.5}W_{0.5}O_6$ powder and liquid components in a ratio of water : monomer : pectin = 70:25:5 with the addition of an ionogenic emulsifier "Ediscan". The completed emulsion was treated using ultrasonic dispergator UZDN-A 650 for 5 minutes. Argon was bubbled into the emulsion for 15 minutes with stirring before the reaction. The reaction was carried out in argon atmosphere. The irradiation was carried out using a visible light LED lamp (white, 30W LED, 6500 K). The emulsion was centrifuged for 30 minutes to separate the catalyst after the reaction, then the organic fraction of the emulsion was extracted with toluene, the aqueous part was dried in vacuum. The catalyst powder was washed in tetrahydrofuran (THF) and chloroform in a Soxhlet extractor and in water under ultrasonic condition. After processing with organic solvents and water, the extracts were separated, the isolated catalyst was dried in vacuum; and all

solutions and the catalyst were analyzed. The solid polymer was isolated from the solution by precipitators and dried. The polymer samples for SEM analysis were dried lyophilically.

2.4 Characterization

Molecular weight characteristics were determined by gel-penetration chromatography (GPC). Organic solutions in tetrahydrofuran were analyzed using a liquid chromatograph "Shimadzu Prominence LC-20VP" with "Tosoh Bioscience" columns (eluent flow rate 0.7 ml/min). Narrow disperse polystyrene standards were used for calibration; a differential refractometer was used as a detector. Water solutions were analyzed using a high-performance liquid chromatograph manufactured by Shimadzu CTO 20A/20A C (Japan) with the LC-Solutions-GPC software module. Separation was performed using a Tosoh Bioscience TSK gel g3000swxl column with a pore diameter of 5 microns and a low-temperature light-scattering detector ELSD-LT II. The eluent was a 0.5 M acetic acid solution, the flow rate was 0.8 ml / min, and narrow disperse dextran standards with a molecular weight (MW) range of 1-410 kDa (Fluca) were used for calibration.

The phase study of the prepared powder was carried out on a Shimadzu XRD-6100 diffractometer (CuKa, λ=1.5418 Å) in the range of 2$\boldsymbol{\theta}$ 10-60˚ with speed of 2 ˚/min. The study of the surface of photocatalyst powder and polymer samples was performed using a scanning electron microscope JSM-IT300 (Jeolltd, Japan) with an electron probe diameter of 5 nm (operating voltage 20 kV), using detectors of low-energy secondary electrons and backscattered electrons in a low vacuum mode to avoid samples charging. The investigation of $RbTe_{1.5}W_{0.5}O_6$ elemental composition before and after polymerization was implemented on energy dispersive X-ray microanalysis method (EDXMA) with detector X-Max^N 20 (Oxford Instruments) using characteristic X-ray lines K_α(C, O) and L_α(Rb, Te, W). Elemental composition of polymer samples was carried out by Vario EL Cube elemental analyzer.

The absorption spectra were recorded using the spectrophotometer “IRPrestige-21” (Shimadzu, Japan), the wavenumber range is 5500-550 cm^{-1}, and the error did not exceed ±0.05 cm^{-1}. Polymer films were prepared on a KBr reflection plate.

The particle size distribution of the prepared $RbTe_{1.5}W_{0.5}O_6$ powder sample by volume and number was determined by laser diffraction method using SALD-2300 analyzer (Shimadzu) (the particle size distributions were calculated by the Fraunhofer theory).

3 Results and Discussion

The process of MMA polymerization was carried out in an aqueous dispersion medium at a temperature of 20-25^{0}C. At the end of the process the organic fraction solvent was added; and the aqueous, organic phases and the catalyst have been analyzed separately.

A polymer (5-10% based on the initial MMA) was isolated from the organic phase using a precipitator, which was analyzed by GPC analysis in a tetrahydrofuran solution. The values of MW and the polydispersity index (PDI) possess the same order as for the MMA photopolymerization using titanium oxide powder [9] (Table 1).

Table 1 Molecular weight parameters of the synthesis product

№		The conditions of polymer allocation	Mn [kDa]	M_W [kDa]	PDI (M_n/M_w)
1		From the organic phase of synthesis	140-145	310-315	2.2
2*	а		381	610	1.6
	б		181	253	1.4
3		After extraction of the oxide with chloroform	200-210	440-450	2.1

*from the publication [9]: a - titanium oxide powder; b - titanium oxide on glass fiber.

However, the MMA polymerization process using $RbTe_{1.5}W_{0.5}O_6$ is characterized by the distinctive feature. SEM analysis and X-ray microanalysis showed that a significant number of polymer fibers are located on the catalyst surface (Fig. 2b).

In order to analyze the bond nature between the polymer and the catalyst and separate the polymer, the powder after reaction was heated at 50^{0}C in a THF solution for 3 hours. However, no noticeable changes of the catalyst surface have been observed; polymer fibers were still presented (Fig. 2c); and the polymer was not detected in the THF solution by the GPC method.

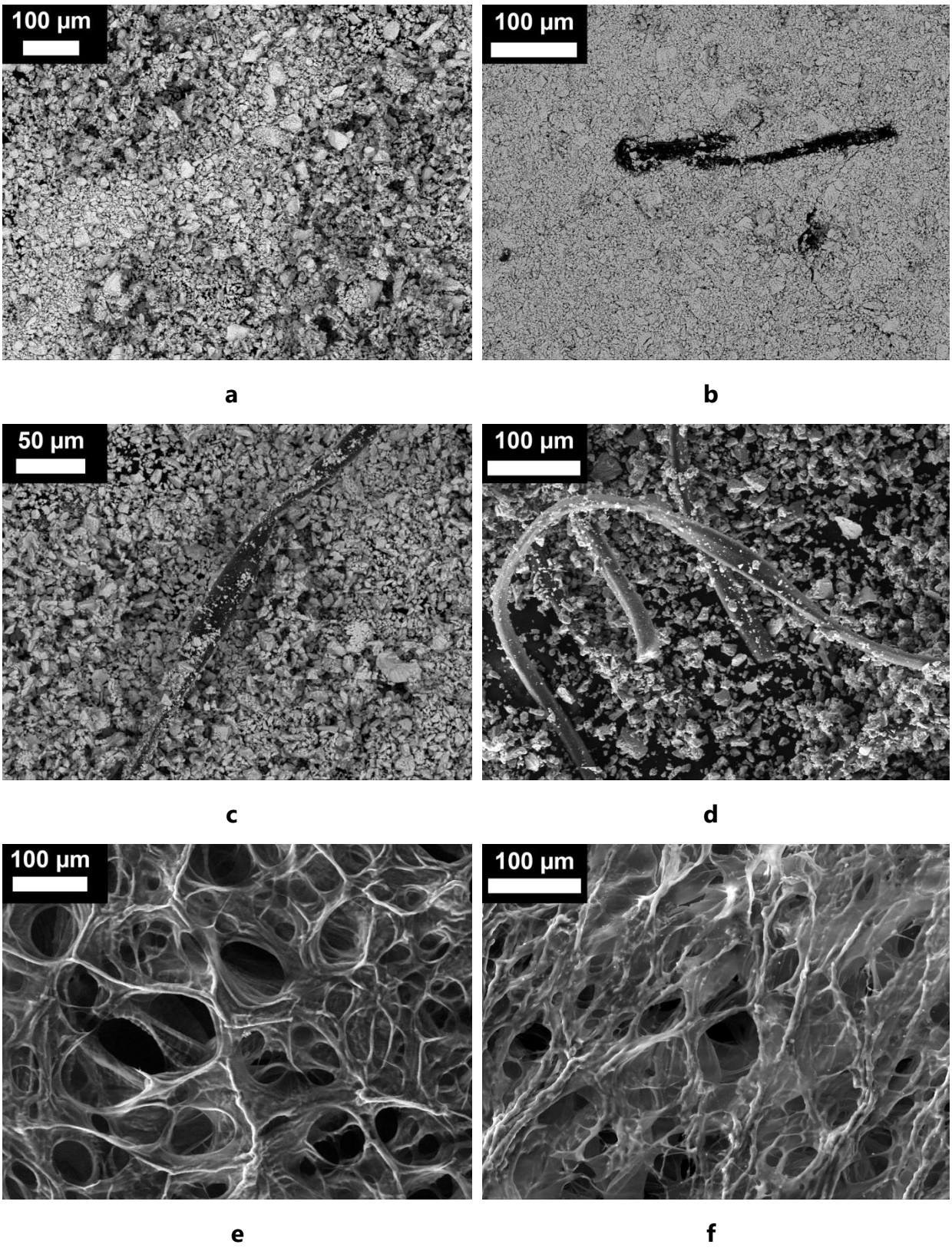

Fig. 2 SEM photographs of $RbTe_{1.5}W_{0.5}O_6$ oxide (**a**) - initial, (**b**) - after polymerization, (**c**) - after heating in tetrahydrofuran solution, (**d**) - after chloroform extraction; and polymer samples: (**e**) - initial pectin, (**f**) – graft copolymer PMMA-pectin

The catalyst after polymerization was subjected to chloroform extraction (temperature 61^0C) in a Soxhlet extractor for 15 hours, but polymer fibers have been still observed on the

catalyst surface (Fig. 2d). Only using ultrasonic bath for 40 minutes at 20^0C in water solution has been allowed to successfully remove the polymer from the powder surface.

Thus, a part of the polymer cannot be washed off from the oxide surface by organic solvents, and it is removed only by ultrasonic treatment due to polymer macromolecules destroying [14-16]. This fact indicates that the macromolecules are bound by a covalent bond to the complex oxide $RbTe_{1.5}W_{0.5}O_6$ surface, so the polymer is grafted onto the oxide surface according to scheme (Fig. 3):

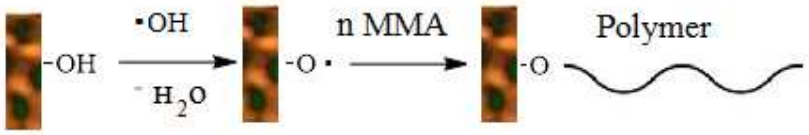

Fig. 3 Scheme of the polymer grafting onto the oxide $RbTe_{1.5}W_{0.5}O_6$ surface

After the catalyst extraction, a solid polymer was isolated in the Soxhlet extractor and studied by GPC, nuclear magnetic resonance (NMR) and infrared (IR) spectroscopy. High-molecular products (Table 1, line 3) with slightly larger values of MW polymer in comparison with the polymer isolated from the organic phase have been detected by the GPC method: Mn~140-145 kDa and 200-210 kDa, respectively. According to NMR spectroscopy data for the polymer, two main signals were observed in the ^{1}H NMR spectrum (Fig. 4a): singlets at 4.69 and 8.10 ppm with an intensity ratio of 1:1. These signals can be attributed to the groups -CH_2OC(O)- and geminal protons at the double bond H_2C=C, respectively. In addition, the weak signals were discovered in the region of 0.95-2.50 ppm and 3.65 ppm that belong to the MMA polymer. The polymethylmethacrylate (PMMA) content according to NMR data does not exceed 10% of the main product. In the ^{13}C NMR spectrum (Fig. 4b), 4 signals belong to the main substance: 62.7 ppm -OCH_2O-; 129.7 ppm H_2C=C; 133.8 ppm C=CH_2 and 165.3 ppm -C(O)O-. The two-dimensional C-H-correlation spectrum (Fig. 4c) confirms that carbon atoms with chemical shifts of 62.7 and 129.7 ppm are directly connected to hydrogen atoms.

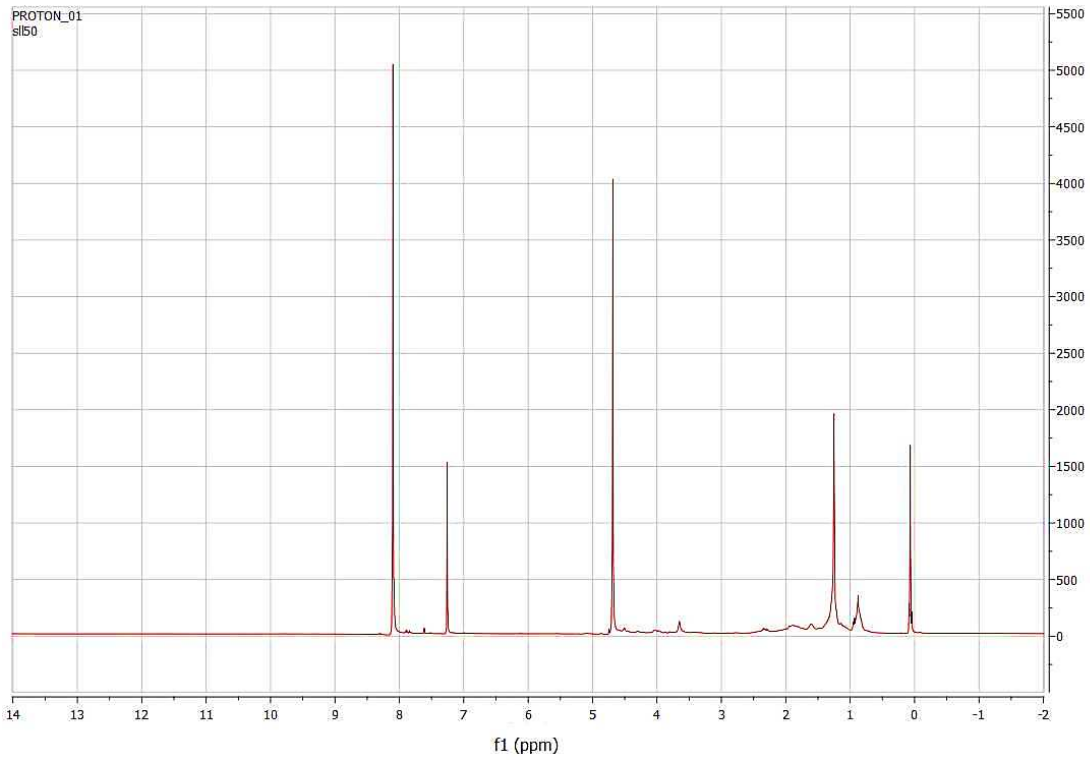

a

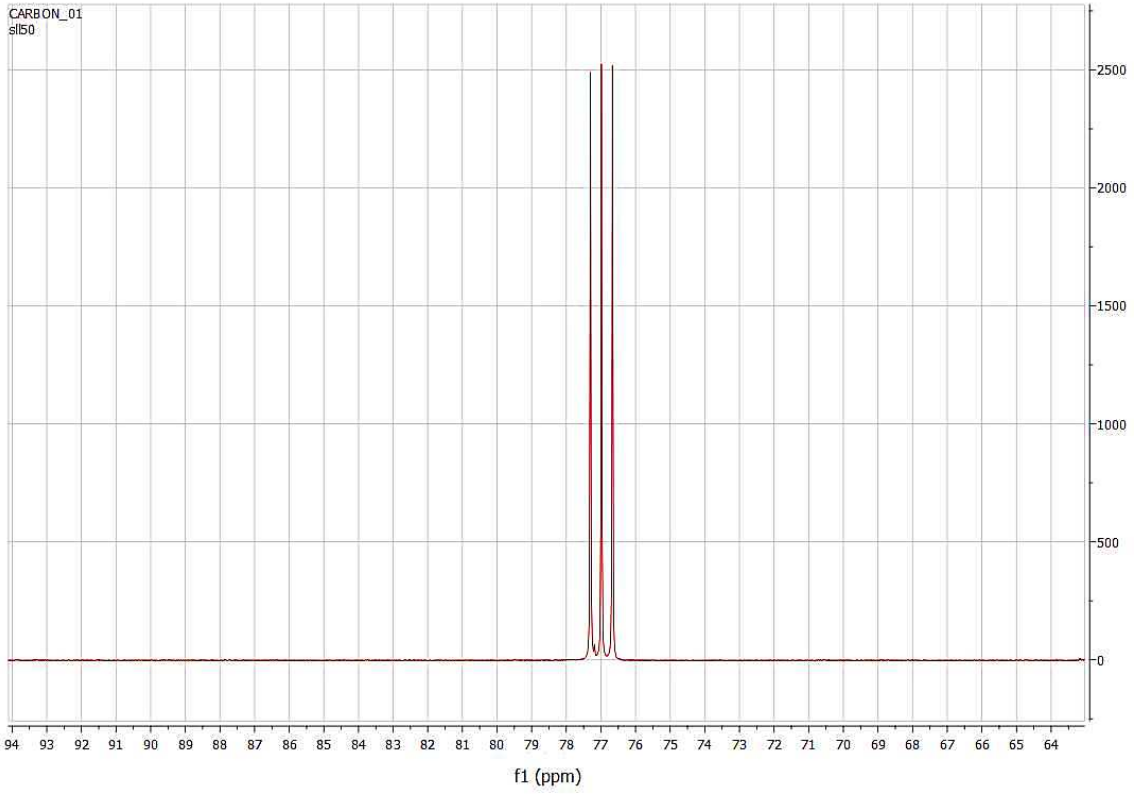

b

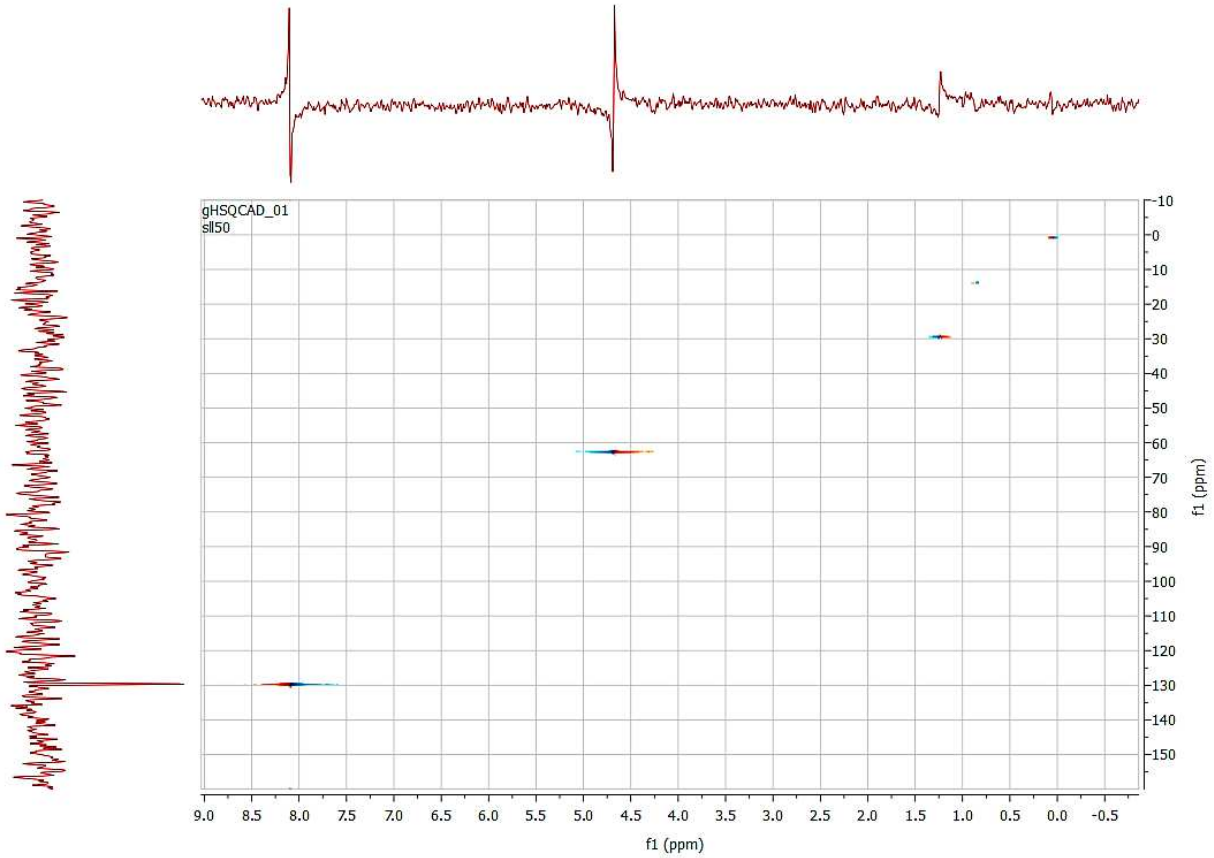

c

Fig. 4 NMR spectroscopy data for the powder isolated from the extract by chloroform: (**a**) - ^{1}H NMR, (**b**) - ^{13}C NMR, (**c**) - C-H correlation

Apparently, the product isolated from chloroform contains not only PMMA, but also other compounds, which can be the result of polymerization of the MMA oxidation products on the oxide catalyst. The analysis of the chloroform solutions using the matrix-assisted laser desorption/ionization (MALDI) method have been confirmed the presence of organic products. The difference in MW of the observed reaction products analyzed by the MALDI method is a multiple of ~ 200 (Fig. 5) and corresponds to the product of oxidative MMA dimerization on the $RbTe_{1.5}W_{0.5}O_6$ oxide surface (Fig. 6), which is able to form a macromolecular chain due to carbon-carbon multiple bonds.

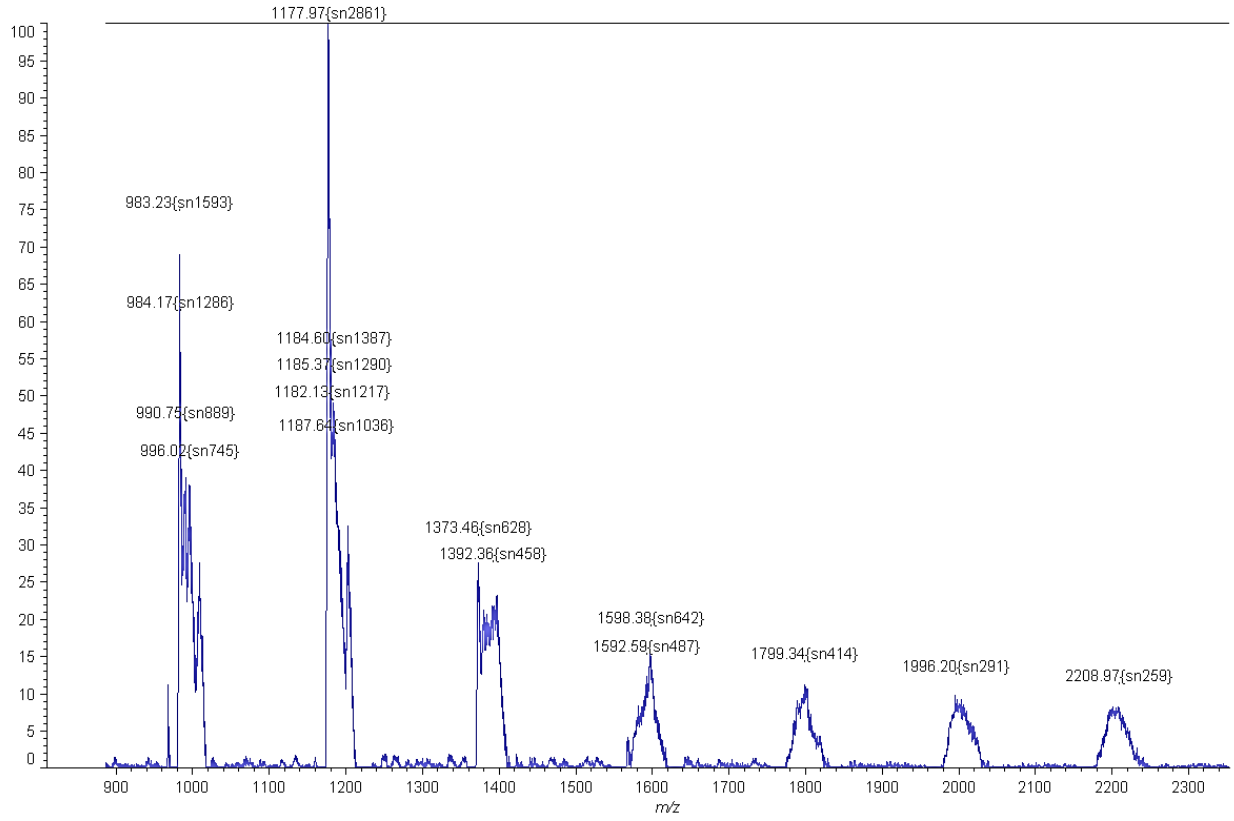

Fig. 5 Mass spectrum MALDI of products in chloroform extract

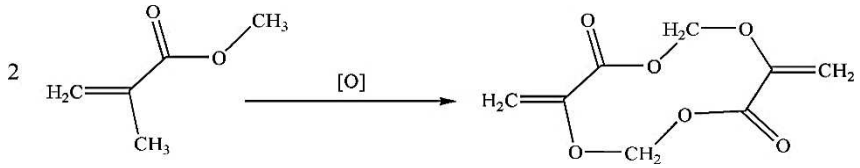

Fig. 6 Scheme of oxidative MMA dimerization on the RbTe1.5W0.5O6 oxide surface

In the IR spectrum of both the PMMA obtained during the azobisisobutyronitrile (AIBN) initiation and the product isolated from chloroform (Fig. 7a), characteristic absorption bands are observed in the region of 1720-1730 cm^{-1}, corresponding to the valence vibrations of the carboxyl group C=O. It confirms the structure of the MMA polymer, presented in the mixture, and the structure of the compound obtained as a result of polymerization of the product of oxidative dimerization of MMA (Fig. 3).

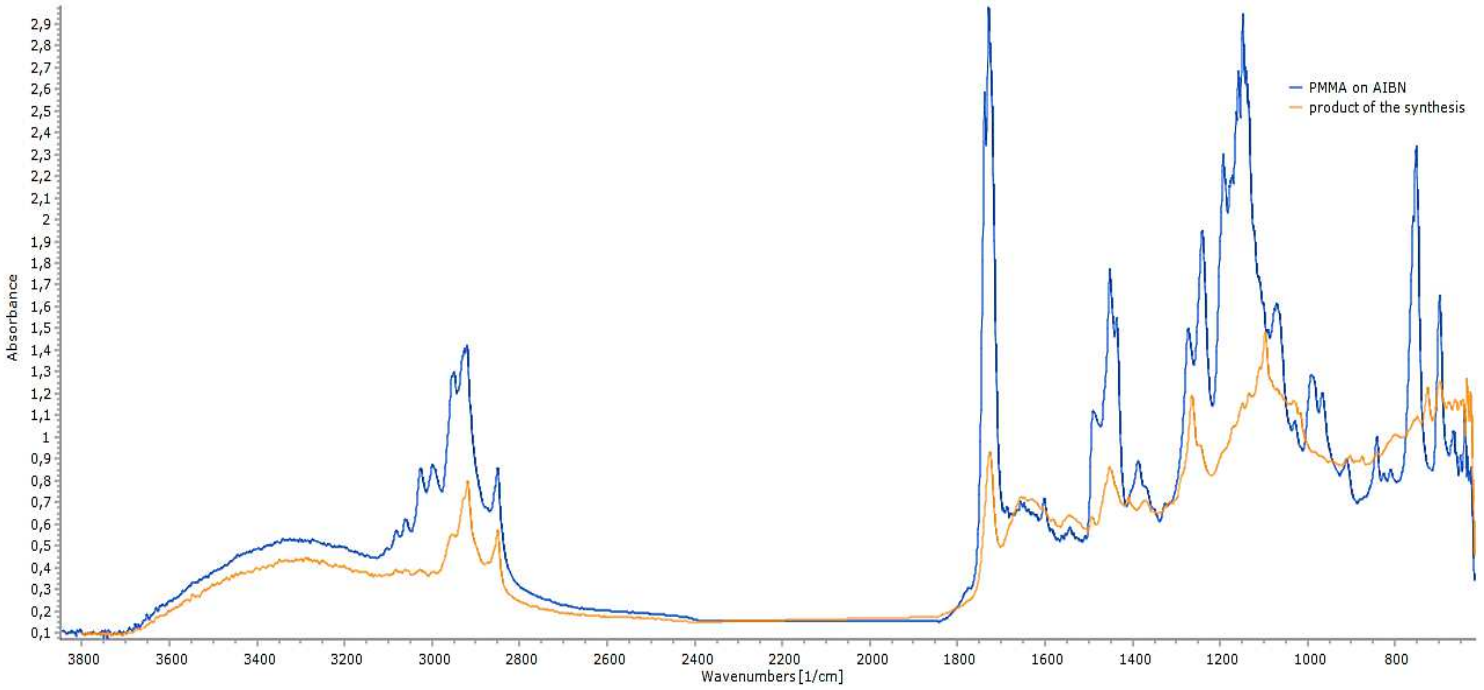

a

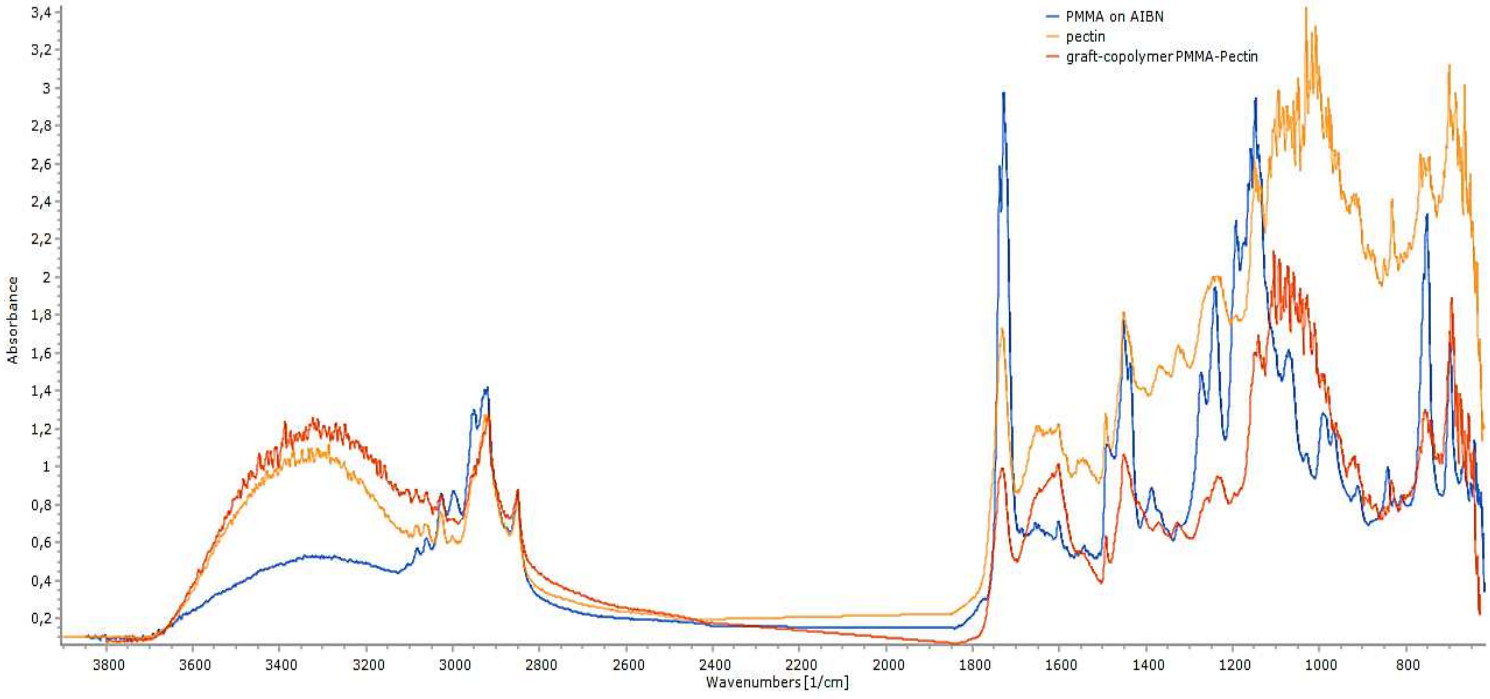

b

Fig. 7 IR spectra: (**a**) comparison of the PMMA obtained during the initiation of DAC with the synthesis product on the photoinitiator;

(**b**) comparison of the graft copolymer PMMA-pectin obtained on the photoinitiator with traditional PMMA and initial pectin

The obtained experimental data allow us to conclude that the transformations of MMA in the reaction mixture apparently take place in several directions:

- PMMA formation in the emulsion due to the initiation of polymerization by a hydroxyl radical (the usual PMMA formation with Mn~ 140-145);
- PMMA formation by grafting on the $RbTe_{1.5}W_{0.5}O_6$ oxide surface, which can be explained by the following reasons. It is well known [17-19] that metal oxides always have OH- groups on the surface. Accordingly, the properties of OH- groups may differ significantly depending on the metal nature. In this case, the hydroxyl radicals formed during photoinitiation can interact with the surface OH- group that lead to appearance a much more stable oxygen-centered radical on the oxide surface, which can also initiate polymerization. The lifetime of the hydroxyl radical is very short, so the polymer formation path due to grafting on the oxide surface becomes preferred. The polymer formed on the surface prevents the release of radicals from the powder surface into the reaction mixture volume;
- The monomer interacts with the complex oxide $RbTe_{1.5}W_{0.5}O_6$ and forms a coordination complex due to double bonds of the monomer and vacant metal orbitals. Coordination of the carbonyl group and the double bond of the monomer [20-22] is equiprobable, and MMA oxidation to a dimer (Fig. 3) by the catalyst $RbTe_{1.5}W_{0.5}O_6$ can be assumed.

The products of the MMA conversion under complex oxide $RbTe_{1.5}W_{0.5}O_6$ irradiation partially allocated by extraction with chloroform in Soxhlet extractor. Extracted products are mixture of PMMA and a polymer product of oxidative dimerization of MMA according to GPC, NMR and mass spectrometry MALDI data.

The presented data confirm the well-known ideas that hydroxyl radicals are very active in the separation reactions of hydrogen atoms from C-H and O-H bonds. Accordingly, they should be highly active against all such bonds, for example, in natural polymers, proteins and polysaccharides. The production of graft copolymers of natural polymers with synthetic polymers is particularly promising for the production of new materials for medicine, including tissue engineering [23-35]. Pectin-containing scaffolds are proved to be a successful basis for the reconstitution of cartilage and bone tissue [36-45]. The effect of the use of various origins pectin on the structural and mechanical properties of the obtained polycomposite frameworks has been studied [46]. Various approaches involving the use of scaffolds made of a wide variety of materials, including synthetic and natural polymers, as well as their copolymers, have been experimentally studied to reconstruct skeletal muscle injuries [39, 41, 47-50].

The research of the photocatalyst $RbTe_{1.5}W_{0.5}O_6$ activity in graft copolymerization of MMA was carried out on the example of pectin polysaccharide.

MMA grafting on pectin was performed under conditions similar to MMA polymerization at 20-25^{0}C. Analysis of the polymer product isolated from the aqueous phase after synthesis indicates the formation of a graft copolymer PMMA-pectin. The product weight from the aqueous phase after synthesis in comparison with the weight of the initial pectin increased by 15-20%. The molecular weight parameters of the copolymer in comparison with the initial pectin have been noticeable changed (Table 2).

Table 2 Molecular weight parameters of pectin and graft copolymer PMMA-pectin

Sample	Mn,kDa	Mw,kDa	PDI (Mw/Mn)	Fraction content in the sample, %
Initial pectin	21.3	21.3	1.00	0.8
	11.6	11.7	1.01	3.1
	0.3	0.4	1.31	96.0
graft copolymer PMMA-pectin	20.6	20.7	1.00	3.8
	11.3	11.4	1.01	10.2
	0.3	0.4	1.27	86.0

The content of the low molecular weight fraction with Mn~0.3 kDa decreased by 10%, while the fraction with MW~11-12 kDa and MW~20-21 kDa increased by 7% and 3%, respectively. Obviously, it is related with the MMA grafting to pectin by the separation of hydrogen atoms from C-H and O-H bonds.

Films of the initial pectin, PMMA and graft copolymer PMMA-pectin were analyzed by IR spectroscopy. Figure 7b shows the obtained IR spectra. The IR spectrum of the pectin film has characteristic absorption bands in the regions 3000-3600 cm^{-1} corresponding to OH- vibrations; 1750-1400 (1750-1730) cm^{-1} corresponding to valence vibrations of the carboxyl group C=O; 1250-1400 cm^{-1} corresponding to OH- vibrations; 1000-1200 and 400-850 cm^{-1} corresponding to pulsation vibrations of pyranose rings. The absorption band in the region of 1720-1730 cm^{-1}, corresponding to the valence vibrations of the carboxyl group C=O, is also characteristic in the IR spectrum of PMMA obtained on AIBN. Comparison of the IR spectrum of the graft copolymer PMMA-pectin with the IR spectra of pectin and PMMA indicates that all the characteristic bands of pectin and PMMA are observed, which is an additional confirmation of the graft copolymer formation.

The SEM analysis revealed morphological differences between the initial pectin and the graft copolymer pectin-PMMA, indicating the inclusion of synthetic polymer fragments in the fibrillar organization of pectin. The pectin sponge has clear outlines of fibrils and formed pores (Fig. 2d), while the picture of the PMMA-pectin graft copolymer sponge clearly shows a more complex structural and topological organization between the pectin fibers (Fig. 2e).

4 Conclusion

It was found that several directions of monomer transformations occur simultaneously in the reaction mixture as a result of radical polymerization of methylmethacrylate in an aqueous emulsion using the complex oxide $RbTe_{1.5}W_{0.5}O_6$ as a photoinitiator under visible light irradiation λ= 400-700 nm. Polymethylmethacrylate is formed in the organic phase because of the initiation of polymerization by a hydroxyl radical, characterized by Mn ~ 140-145 kDa. Moreover, oxygen-centered radicals are formed on the complex oxide $RbTe_{1.5}W_{0.5}O_6$ surface, which grafts polymer macromolecules onto the photocatalyst surface by the interaction of hydroxyl radicals with OH groups. At the same time, the monomer interacts with the complex oxide $RbTe_{1.5}W_{0.5}O_6$ and forms a coordination complex by the double bonds, while its oxidation occurs to a cyclic dimer with terminal double bonds (Fig. 8):

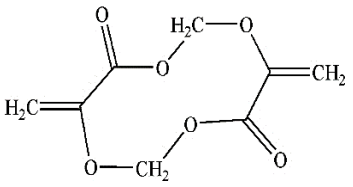

Fig. 8 Structure of the cyclic dimer with terminal double bonds as a result of monomer oxidation

The high activity of the hydroxyl radical is confirmed by grafting the polymer product onto the surface of a natural polymer-pectin polysaccharide with the graft copolymer formation. A new structural and topological organization of the graft copolymer PMMA-pectin in comparison with the original pectin was established by the SEM method comparing the samples sponges. This morphological feature is the basis for conducting research on its properties as a material for the scaffolds. The absence of initiator fragments with organic nature, which is characteristic of polymers with organic material initiation, is important in this case.

The results of the research were obtained using modern methods of physical and chemical analysis: GPC, IR, NMR, SEM etc.

References

1. W. Mao, L. Zhang, T. Wang, Y. Bai, Y. Guan, Fabrication of highly efficient Bi2WO6/CuS composite for visible-light photocatalytic removal of organic pollutants and Cr(VI) from wastewater. Front. Environ. Sci. Eng. **15**(4), 52 (2021)

2. J. Wang, S. Sun, R. Zhou, Y. Li, Z. He, H. Ding, D. Chen, W. Ao, Synthesis, modification and photocatalytic applications of $ZnIn_2S_4$. J. Mater. Sci. Technol. **78**, 1-19 (2021)
3. W. Wang, X. Wang, L. Gan, X. Ji, Z. Wu, R. Zhang, All solid-state Z-scheme $BiVO_4$−$Bi_6O_6(OH)_3(NO_3)_3$ heterostructure with prolonging electron-hole lifetime for enhanced photocatalytic hydrogen and oxygen evolution. J. Mater. Sci. Technol. **77**, 117-125 (2021)
4. M.Z. Hussain, Z. Yang, B.V.D. Linden, Z. Huang, Q. Jia, E. Cerrato, R.A. Fischer, F. Kapteijn, Y. Zhu, Y. Xia, Surface functionalized N-C-TiO_2/C nanocomposites derived from metal-organic framework in water vapour for enhanced photocatalytic H_2 generation. J. Energy Chem. **57**, 485-495 (2021)
5. K. Khan, L. Xu, M. Shi, J. Qu, X. Tao, Z. Feng, C. Li, R. Li, Surface assembly of cobalt species for simultaneous acceleration of interfacial charge separation and catalytic reactions on $Cd_{0.9}Zn_{0.1}S$ photocatalyst. Chin. J. Catal. **42**(6), 1004-1012 (2021)
6. D.G. Fukina, E.V. Suleimanov , A.V. Boryakov, S.Yu Zubkov, A.V. Koryagin, N.S. Volkova , A.P. Gorshkov, Structure analysis and electronic properties of $ATe^{4+}_{0.5}Te^{6+}_{1.5-x}M^{6+}_xO_6$ (A=Rb, Cs, M^{6+}=Mo, W) solid solutions with β-pyrochlore structure. J. Solid State Chem. **293**, 121787 (2021)
7. D. Zhang, C. Bi, Z. Zong, Y. Fan, Three different Co(II) Metal–Organic frameworks based on 4,4′-Bis(imidazolyl)diphenyl ether: syntheses, crystal structure and photocatalytic properties. J. Inorg. Organomet. Polym. Mater. **30**, 5148–5156 (2020)
8. W.C. Chanu, A. Gupta, M.K. Singh, O.P. Pandey, Group V elements (V, Nb and Ta) doped CeO_2 particles for efficient photo-oxidation of methylene blue dye. J. Inorg. Organomet. Polym. Mater. (2020). https://doi.org/10.1007/s10904-020-01822-0
9. H. Wang, J.-R. Zhang, X.-F. Wu, C. Wang, Y. Li, L.-J. Ci, Y.-N. Jia1, T.-L. Chang, X.-T. Liu, Y.-X. Fun, Study on Ag_2WO_4/g-C_3N_4 nanotubes as an efficient photocatalyst for degradation of rhodamine B. J. Inorg. Organomet. Polym. Mater. **30**, 4847–4857 (2020)
10. N. Ali, F. Ali, R. Khurshid, Ikramullah, Z. Ali, A. Afzal, M. Bilal, H.M.N. Iqba, I. Ahmad, TiO_2 nanoparticles and epoxy-TiO_2 nanocomposites: a review of synthesis, modification strategies, and photocatalytic potentialities. J. Inorg. Organomet. Polym. Mater. **30**, 4829–4846 (2020)
11. T. Tavakoli-Azar, A.R. Mahjoub, M.S. Sadjadi, N. Farhadyar, M.H. Sadr, Synthesis and characterization of a perovskite nanocomposite of $CdTiO_3$@S with orthorhombic structure: investigation of photoluminescence properties and its photocatalytic

performance for the degradation of congo red and crystal violet under sunlight. J. Inorg. Organomet. Polym. Mater. **30**, 4858–4875 (2020)

12. E. Lobry, A.S. Bt Bah, L. Vidal, E. Oliveros, A.M. Braun, A. Criqui, A. Chemtob, Colloidal and supported TiO_2: toward nonextractable and recyclable photocatalysts for radical polymerizations in aqueous dispersed media. Macromol. Chem. Phys. **217**, 2321−2329 (2016)
13. F. Mouslia, A. Chaouchib, S. Hocineb, A. Lamouric, M.R. Vilarc, A. Kadria, M.M. Chehimic, Diazonium-modified TiO_2/polyaniline core/shell nanoparticles. Structural characterization, interfacial aspects and photocatalytic performances. Appl. Surf. Sci. **465,** 1078–1095 (2019)
14. D.G. Fukina, E.V. Suleimanov, G.K. Fukin, A.V. Boryakov, S.Y. Zubkov, L.A. Istomin, Crystal structure features of the mixed-valence tellurium β-pyrochlores: $CsTe_{1.625}W_{0.375}O_6$ and $RbTe_{1.5}W_{0.5}O_6$. J. Solid State Chem. **286**, 121276 (2020)
15. C. Hernandez, S. Gulati, G. Fioravanti, P. Stewart, A. Exner, On the fate of mesh-stabilized lipid nanobubbles after destruction with ultrasound (Conference Paper). IEEE IUS, 80928532017 (2017)
16. J. Li, B. Li, P. Geng, A.-X. Song, J.-Y. Wu, Ultrasonic degradation kinetics and rheological profiles of a food polysaccharide (konjac glucomannan) in water. Food Hydrocolloids. **70**, 14-19 (2017)
17. W. Chen, X. Gao, H. Xu, Y. Cai, J. Cui, Influence of extracellular polymeric substances (EPS) treated by combined ultrasound pretreatment and chemical re-flocculation on water treatment sludge settling performance. Chemosphere **170**, 196-206 (2017)
18. C. Li, S. Yang, R. Bian, Y. Tan, X. Dong, N. Zhu, X. He, S. Zheng, Z. Sun, Clinoptilolite mediated activation of peroxymonosulfate through spherical dispersion and oriented array of $NiFe_2O_4$: Upgrading synergy and performance. J. Hazard. Mater. **407**, 124736 (2021)
19. J. Lee, J. Hwang, H. Park, T. Sekino, W.-B. Kim, Preparation of ultra-thin TiO_2 shell by peroxo titanium complex (PTC) solution-based green surfacemodification, and photocatalytic activity of homo-core/shell TiO_2. Appl. Surf. Sci. **540**, 148399 (2021)
20. W. Zhao, L. Yan, H. Gu, Z. Li, Y. Wang, Q. Luo, Y. Yang, X. Liu, H. Wang, C.-Q. Ma, Zinc oxide coated carbon dot nanoparticles as electron transport layer for inverted polymer solar cells. ACS Appl. Energy Mater. **3**(11), 11388-11397 (2020)
21. D.F Grishin, L.L Semyonycheva, Problems of control of the reactivity of macroradicals and the growth of polymer chains. Russ. Chem. Rev. 70(5), 486-509 (2001)
22. V.A. Kabanov, V.P. Zubov, Yu.D. Semchikov, Complex-radical polymerization (Khimiya, Moscow, 1987) p. 254

23. V.A. Kabanov, Radical coordination polymerization. J. Polym. Sci. Polymer Symp. **18**(67), 17-34 (1980)
24. N. Iqbal, A.S. Khan, A. Asif, M. Yar, J.W. Haycock, I. Rehman, Recent concepts in biodegradable polymers for tissue engineering paradigms. Int. Mater. Rev. **64**(2), 91–126 (2018)
25. A.A. Ivanov, O.P. Popova, T.I. Danilova, A.V. Kuznetsova, Strategies for selecting and use of scaffolds in bioengineering. Biol. Bul. Rev. **139**(2), 196–205 (2019)
26. Q. Huang, Y. Zou, M.C. Arno, S. Chen, T. Wang, J. Gao, A.P. Dove, J. Du, Hydrogel scaffolds for differentiation of adipose-derived stem cells. Chem. Soc. Rev. **46**(20), 6255–6275 (2017)
27. S. Chen, Y. Li, L. Xie, S. Liu, Y. Fan, C. Fang, X. Zhang, Jb. Quan, L. Zuo, Thermosensitive chitosan-collagen composite hydrogel loaded with basic fibroblast growth factor retards ventricular remodeling after myocardial infarction in mice. Chin. J. Tissue Eng. Res. **25**(16), 2472-2478 (2021)
28. M. Castilho, G. Hochleitner, W. Wilson, B. Rietbergen, P.D. Dalton, J. Groll, J. Malda, K. Ito, Mechanical behavior of a soft hydrogel reinforced with three-dimensional printed microfibre scaffolds. Sci. Rep. **8**(1), 1–10 (2018)
29. H.-J. Jiang, J. Xu, Z.-Y. Qiu, X.-L. Ma, Z.-Q. Zhang, X.-X. Tan, Y. Cui, F.-Z. Cui, Mechanical properties and cytocompatibility improvement of vertebroplasty PMMA bone cements by incorporating mineralized collagen. Materials. **8**, 2616-2634 (2015)
30. M. Vedhanayagam, S. Ananda, B.U. Nair, K.J. Sreeram, Polymethyl methacrylate (PMMA) grafted collagen scaffold reinforced by PdO-TiO_2 nanocomposites. Mater. Sci. Eng., C. 110378 (2019)
31. B. Carrion, M.F. Souzanchi, V.T. Wang, G. Tiruchinapally, A. Shikanov, A.J. Putnam, R.M. Coleman, The synergistic effects of matrix stiffness and composition on the response of chondroprogenitor cells in a 3D precondensation microenvironment. Adv. Healthcare Mater. **5**(10), 1192-1202 (2016)
32. J.L.A. Del Barrio, F. Arnalich-Montiel, M. Chiesa, I. García-Tuñón, M.P. De Miguel, G.G. Ferrer, J.L.G. Ribelles, C.M. Antolinos-Turpín, J.A. Gómez-Tejedor, N. Garagorri, N. Briz, J. Fernandez-Delgado, M.S.-T. Valls, C.C. Botella, L. Bataille, A. Rodriguez, J.L. Alió, Biointegration of corneal macroporous membranes based on poly(ethyl acrylate) copolymers in an experiental animal model. J. Biomed. Mater. Res., Part A. **103**(3), 1106-1118 (2015)

33. O. Bas, E.M. De-Juan-Pardo, M.P. Chhaya, F.M. Wunner, J.E. Jeon, T.J. Klein, D.W. Hutmacher, Enhancing structural integrity of hydrogels by using highly organised melt electrospun fibre constructs. Eur. Polym. J. **72**, 451-463 (2015)
34. S. Fujisawa, Y. Kadoma, Tri-n-butylborane/water complex-mediated copolymerization of methyl methacrylate with proteinaceous materials and proteins. Polymers. **2**, 575-595 (2010)
35. Y.L. Kuznetsova, E.A. Morozova, A.S. Vavilova, A.V. Markin, O.N. Smirnova, N.S. Zakharycheva, D.V. Lyakaev, L.L. Semenycheva, Synthesis of biodegradable grafted copolymers of gelatin and polymethyl methacrylate // Pol. Sci.. Ser. D. **13**(4) 453-459 (2020)
36. Y.L. Kuznetsova, K.S. Sustaeva, A.S. Vavilova, A.V. Mitin, L.L. Semenycheva, Tributylborane in the synthesis of graft-copolymers of gelatin and acrylamide. J. Organomet. Chem. **924**, 121431 (2020)
37. M. Sumathra, D. Govindaraja, M. Jeyarajb, A.A. Arfajc , M.A. Munusamyc , S.S. Kumard, M. Rajana, Sustainable pectin fascinating hydroxyapatite nanocomposite scaffolds to enhance tissue regeneration. Sustainable Chem. Pharm. **5**, 46–53 (2017)
38. S. Raghav, S. Nehra, D. Kumar, Biopolymer scaffold of pectin and alginate for the application of health hazardous fluoride removal studies by equilibrium adsorption, kinetics and thermodynamics. J. Mol. Liq. **284**, 203–214 (2019)
39. A.F. Martins, V. Jessi, T. Wigmosta, M. Hedayati, M.M. Reynolds, K.C. Popat, M.J. Kipper, Chitosan/iota-carrageenan and chitosan/pectin polyelectrolyte multilayer scaffolds with antiadhesive and bactericidal properties. Appl. Surf. Sci. **502**, 144282 (2020)
40. F.C. Bombaldi de Souza, R. F. Bombaldi de Souza, B. Drouin, D. Mantovani, A.M. Moraes, Comparative study on complexes formed by chitosan and different polyanions: Potential of chitosan-pectin biomaterials as scaffolds in tissue engineering. Int. J. Biol. Macromol. **132**, 178–189 (2019)
41. S. P. Mallick, B. N. Singh, A. Rastogi, P. Srivastava, Design and evaluation of chitosan/poly(L-lactide)/pectin based composite scaffolds for cartilage tissue regeneration. Int. J. Biol. Macromol. **112**(2017), 909–920 (2018)
42. M. Ghorbani, L. Roshangar, J. Soleimani Rad, Development of reinforced chitosan/pectin scaffold by using the cellulose nanocrystals as nanofillers: An injectable hydrogel for tissue engineering. Eur. Polym. J. **130**, 109697 (2020)
43. F. Ahadi, S. Khorshidi, A. Karkhaneh, A hydrogel/fiber scaffold based on silk fibroin/oxidized pectin with sustainable release of vancomycin hydrochloride. Eur. Polym. J. **118**, 265–274 (2019)

44. P.T.S. Kumar, C. Ramya, R. Jayakumar, S. Nair, V. Kumar, V.K. Lakshmanan, Drug delivery and tissue engineering applications of biocompatible pectin-chitin/nano $CaCO_3$ composite scaffolds. Colloids Surf., B. **106**, 109–116 (2013)
45. J.G. Martins, S.E.A. Camargo, T.T. Bishop, K.C. Popat, M.J. Kipper, A.F. Martins, Pectin-chitosan membrane scaffold imparts controlled stem cell adhesion and proliferation. Carbohydr. Polym. **197**, 47–56 (2018)
46. N. Ninan, M. Muthiah, I.-K. Park, A. Elain, S. Thomas, Y. Grohens, Pectin/carboxymethyl cellulose/microfibrillated cellulose composite scaffolds for tissue engineering. . Carbohydr. Polym. **98**(1), 877–885 (2013)
47. M. Moslemi, Reviewing the recent advances in application of pectin for technical and health promotion purposes: From laboratory to market. Carbohydr. Polym. 117324 (2020)
48. Y. Gao, J.U. Fangel, W.G.T. Willats, M.A. Vivier, J. P. Moore, Dissecting the polysaccharide-rich grape cell wall matrix using recombinant pectinases during winemaking. Carbohydr. Polym. **152**, 510–519 (2016)
49. N. Işıklan, Ş. Tokmak, Development of thermo/pH-responsive chitosan coated pectin-graft-poly(N,N-diethyl acrylamide) microcarriers. Carbohydr. Polym. **218**, 112–125 (2019)
50. N. Işıklan, S. Polat, Synthesis and characterization of thermo/pH-sensitive pectin-graft-poly(dimethylaminoethyl methacrylate) coated magnetic nanoparticles. Int. J. Biol. Macromol. **164**, 4499–4515 (2020)

Figures

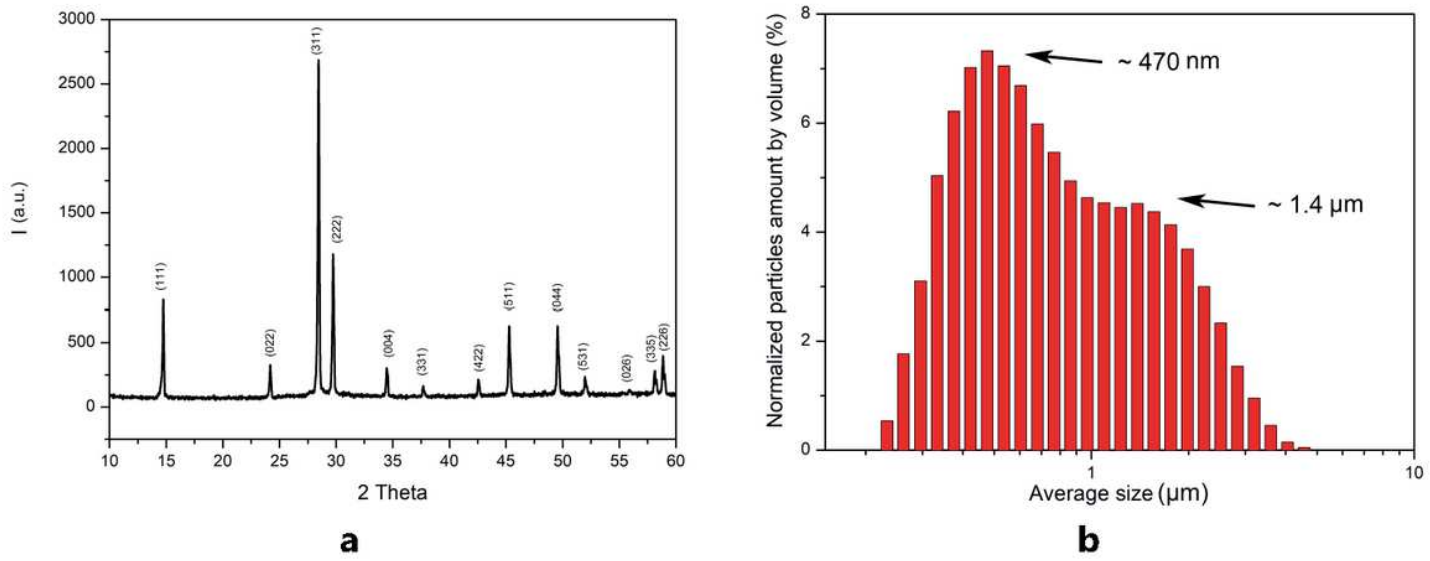

Figure 1

X-ray powder diffraction pattern (a) and size particles distribution by volume over the size of RbTe1.5W0.5O6 (b)

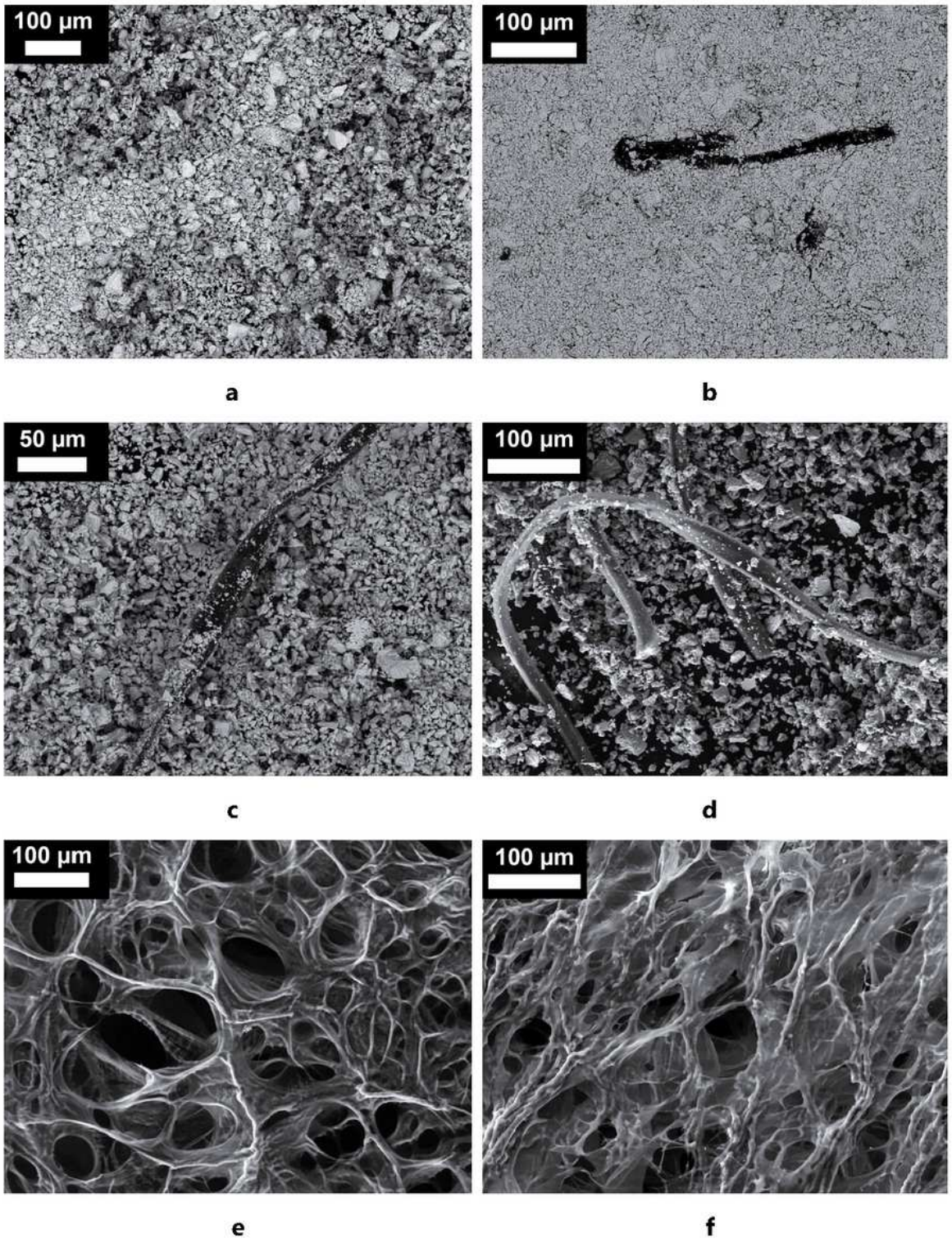

Figure 2

SEM photographs of RbTe1.5W0.5O6 oxide (a) - initial, (b) - after polymerization, (c) - after heating in tetrahydrofuran solution, (d) - after chloroform extraction; and polymer samples: (e) - initial pectin, (f) – graft copolymer PMMA-pectin

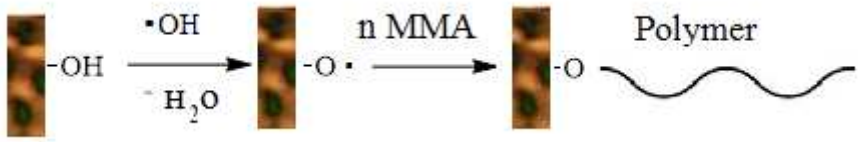

Figure 3

Scheme of the polymer grafting onto the oxide RbTe1.5W0.5O6 surface

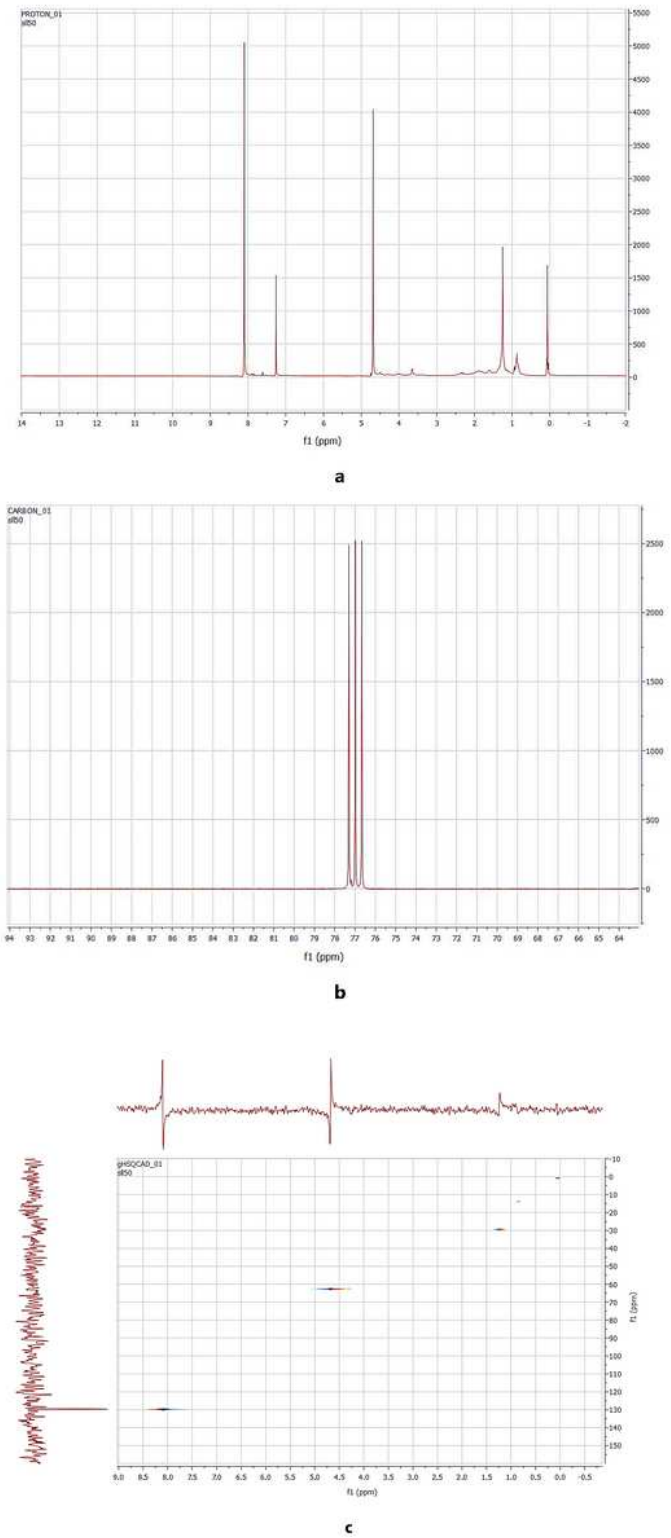

Figure 4

NMR spectroscopy data for the powder isolated from the extract by chloroform: (a) - 1H NMR, (b) - 13C NMR, (c) - C-H correlation

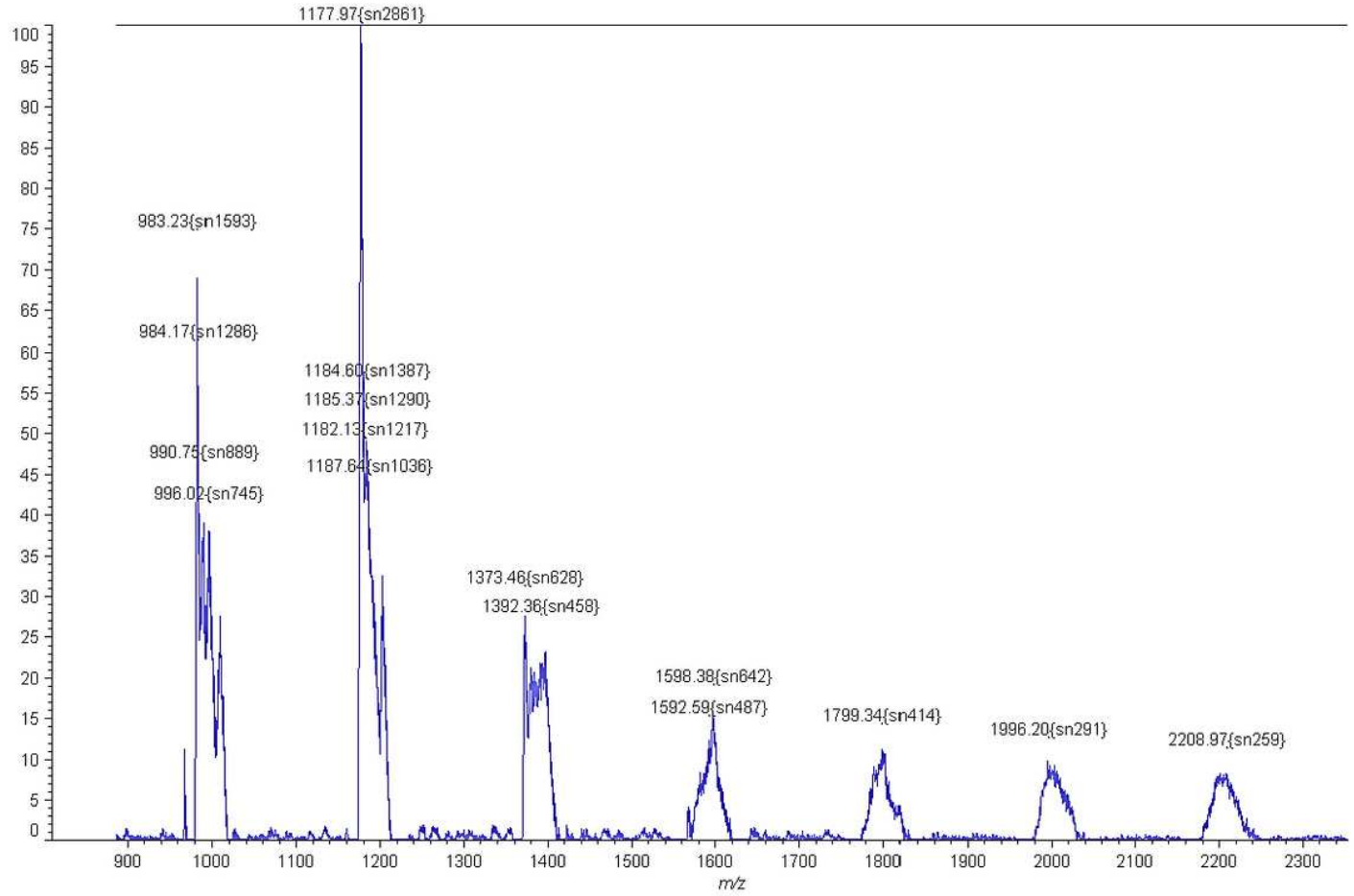

Figure 5

Mass spectrum MALDI of products in chloroform extract

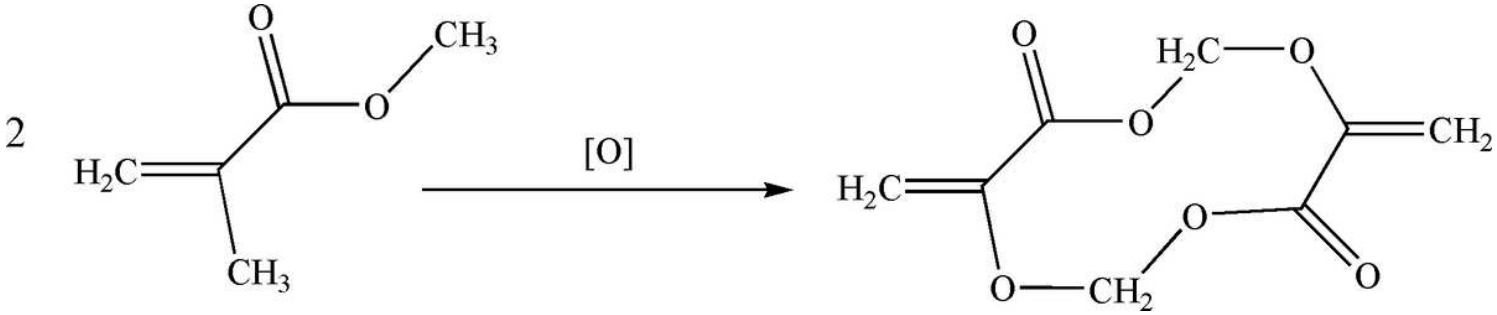

Figure 6

Scheme of oxidative MMA dimerization on the RbTe1.5W0.5O6 oxide surface

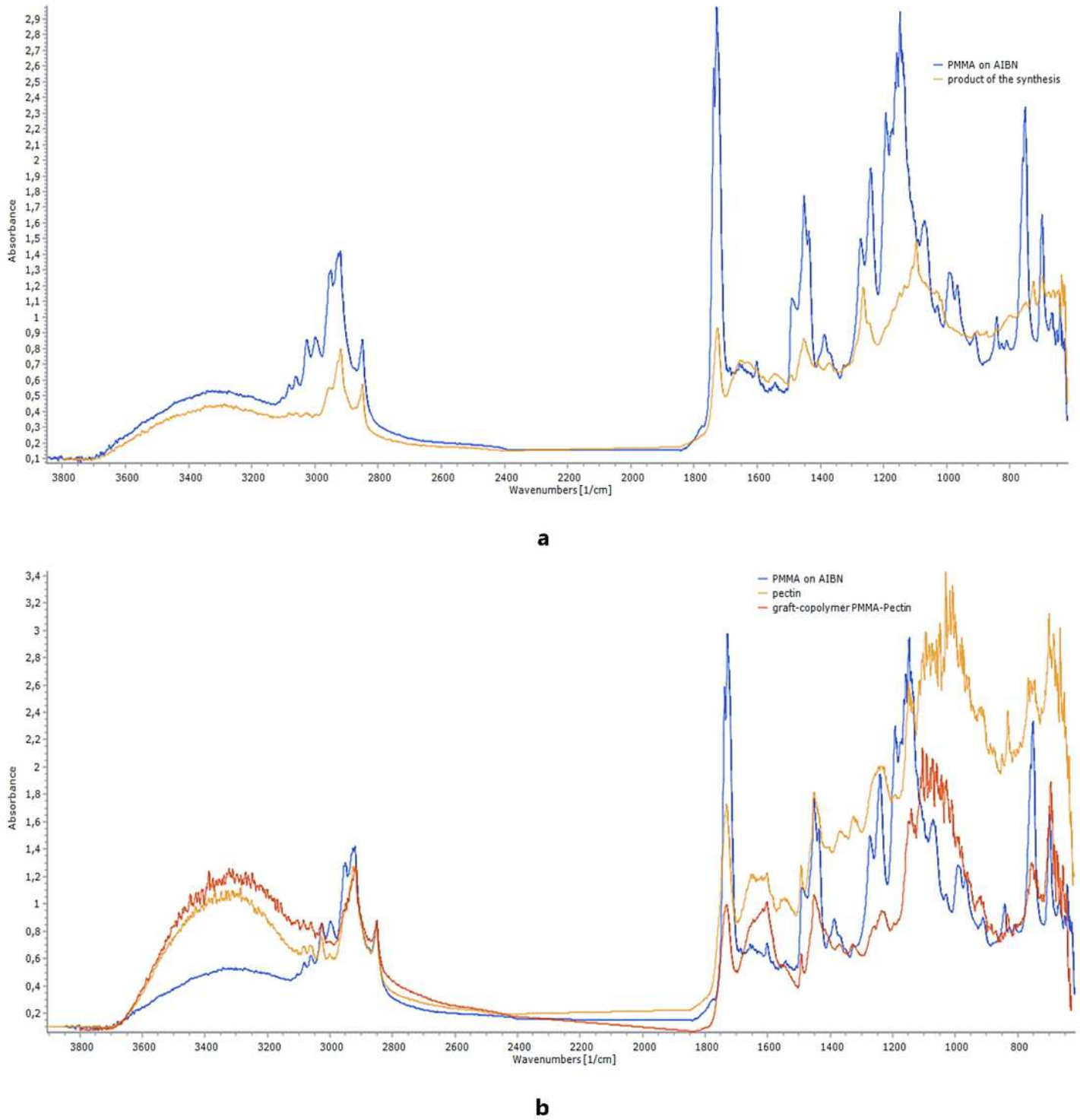

Figure 7

IR spectra: (a) comparison of the PMMA obtained during the initiation of DAC with the synthesis product on the photoinitiator; (b) comparison of the graft copolymer PMMA-pectin obtained on the photoinitiator with traditional PMMA and initial pectin

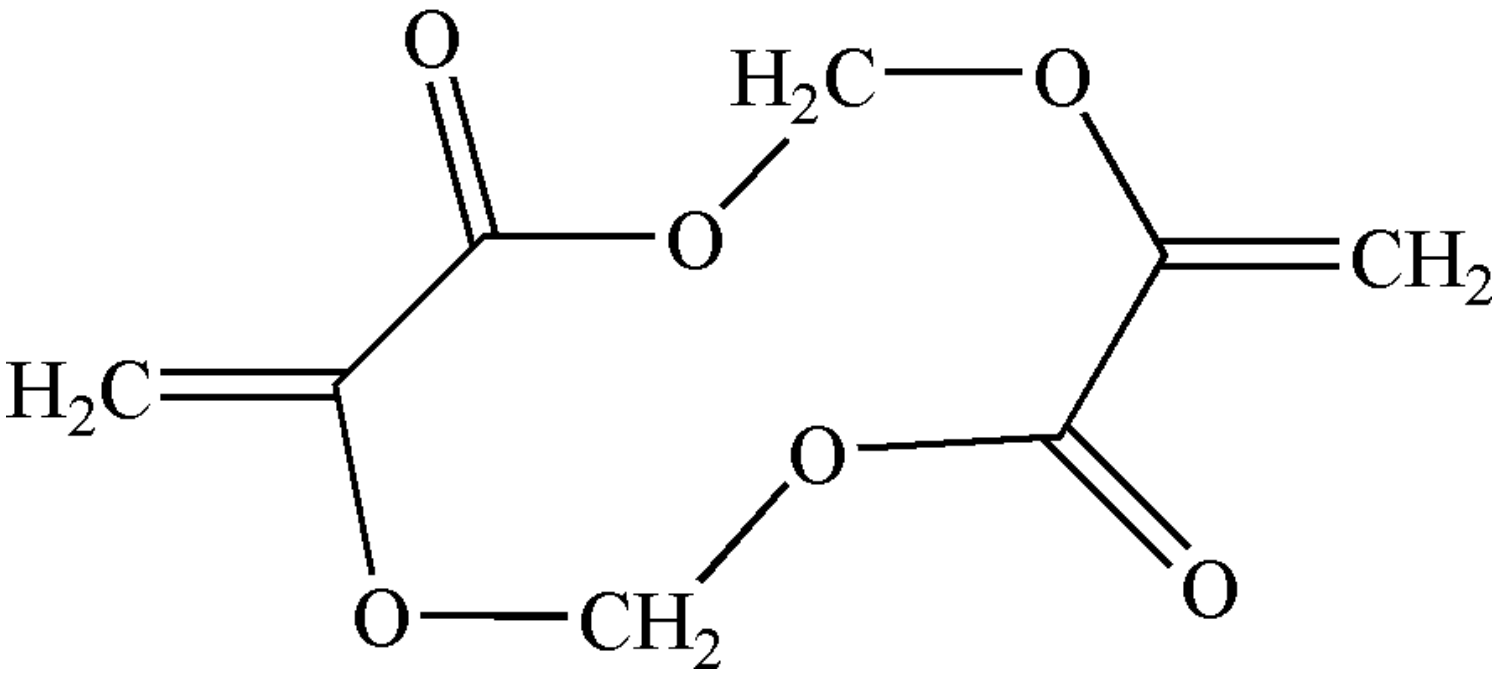

Figure 8

Structure of the cyclic dimer with terminal double bonds as a result of monomer oxidation